

Transcriptome profiling of the newborn mouse brain after hypoxia–reoxygenation: hyperoxic reoxygenation induces inflammatory and energy failure responsive genes

Embjørg J. Wollen¹, Yngve Sejersted^{1,2}, Marianne S. Wright¹, Anna Madetko-Talowska³, Mirosław Bik-Multanowski³, Przemko Kwinta⁴, Clara-Cecilie Günther⁵, Ståle Nygård⁶, Else Marit Løberg⁷, Martin B. Ystgaard¹, Jacek J. Pietrzyk⁴ and Ola D. Saugstad¹

BACKGROUND: Supplemental oxygen used during resuscitation can be detrimental to the newborn brain. The aim was to determine how different oxygen therapies affect gene transcription in a hypoxia–reoxygenation model.

METHODS: C57BL/6 mice ($n = 56$), postnatal day 7, were randomized either to 120 min of hypoxia 8% O₂ followed by 30 min of reoxygenation with 21, 40, 60, or 100% O₂, or to normoxia followed by 30 min of 21 or 100% O₂. Affymetrix 750k expression array was applied with RT-PCR used for validation. Histopathology and immunohistochemistry 3 d after hypoxia–reoxygenation compared groups reoxygenated with 21 or 100% O₂ with normoxic controls ($n = 22$).

RESULTS: In total, ~81% of the gene expression changes were altered in response to reoxygenation with 60 or 100% O₂ and constituted many inflammatory-responsive genes (i.e., *C5ar2*, *Stat3*, and *Ccl12*). Oxidative phosphorylation was down-regulated after 60 or 100% O₂. Iba1⁺ cells were significantly increased in the striatum and hippocampal CA1 after both 21 and 100% O₂.

CONCLUSION: In the present model, hypoxia–reoxygenation induces microglial accumulation in subregions of the brain. The transcriptional changes dominating after applying hyperoxic reoxygenation regimes include upregulating genes related to inflammatory responses and suppressing the oxidative phosphorylation pathway.

Perinatal asphyxia is a major cause of mortality and morbidity in the newborn (1), and efficient resuscitation is required to restore oxygenation and adequate perfusion of the brain. Brain injury following birth asphyxia is related to both hypoxic insult and reoxygenation. Hallmarks of hypoxia–reoxygenation injury include both a decrease in high-energy phosphates due to impaired oxidative phosphorylation (2) and excessive generation of reactive oxygen species. The developing

brain is susceptible to reactive oxygen species–mediated injury due to imbalanced brain antioxidant defense, neuronal membranes rich in polyunsaturated fatty acids, a high rate of oxygen consumption, and high availability of free iron as reviewed in refs. (3–5). Together with a limited threshold for oxidative stress, central nervous system immaturity also provides for a more rapid accumulation of microglia, differences in release of cytokine and chemokine, and a developing complement system, all of which make inflammation an important contributor to both injury and repair after a hypoxic insult (4,6). The developing brain can be exposed to both hypoxia and subsequent hyperoxia in a resuscitation situation. Hyperoxic reperfusion after hypoxia or hypoxia–ischemia (HI) can induce inflammation (7), neuronal damage (8,9), and cell death (10).

Studies have demonstrated that air is as efficient as 100% oxygen for resuscitating the asphyxiated newborn (11,12), and experimental and clinical studies have revealed detrimental effects of 100% oxygen (8). Importantly, mortality is reduced in neonates resuscitated with air compared with 100% oxygen (13). However, there is to date no consensus regarding which fraction of inspired oxygen (FiO₂) to use during resuscitation of the preterm newborn (14). Most of the preterm births happen in the late stage (gestational age 32–36 wk), and these children have increased mortality compared with the term infants (15). The brain of the late preterm is immature compared with the term infant in regard to the development of sulci, synapses, dendrites, microglia, astrocytes, axons, and oligodendrocytes, and the weight of the brain is only 60% that of term infants (15). DNA microarray technology enables large-scale analysis of gene expression patterns. We hypothesized that the use of supplemental oxygen during reoxygenation would induce differential gene expression and pathways as compared with the use of air. To identify oxygen-responsive molecular pathways after hypoxia, we analyzed the transcriptome in late premature mouse brain tissue after a hypoxia–reoxygenation event using

¹Department of Pediatric Research, Clinic of Women and Child Health, Oslo University Hospital, Rikshospitalet, University of Oslo, Oslo, Norway; ²Department of Microbiology and CMBN, University of Oslo, Oslo University Hospital, Rikshospitalet, Oslo, Norway; ³Department of Medical Genetics, Faculty of Medicine, Polish-American Children's Hospital, Jagiellonian University, Krakow, Poland; ⁴Department of Pediatrics, Faculty of Medicine, Polish-American Children's Hospital, Jagiellonian University, Krakow, Poland; ⁵Norwegian Computing Center, Oslo, Norway; ⁶Bioinformatics Core Facility, Institute for Medical Informatics, University of Oslo, Oslo University Hospital, Oslo, Norway; ⁷Department of Pathology, Oslo University Hospital, Ullevaal, Oslo, Norway. Correspondence: Embjørg J. Wollen (ewollen@rr-research.no)

Received 19 April 2013; accepted 13 September 2013; advance online publication 29 January 2014. doi:10.1038/pr.2013.249

different FiO_2 . Histopathology and immunohistochemistry (IHC) were performed to validate the hypoxia–reoxygenation model.

RESULTS

Histopathological and Immunohistochemical Analysis

To validate the hypoxia–reoxygenation model, hematoxylin and eosin (HE) staining and immunohistochemical analysis were performed on postnatal day 7 (P7) mice from four litters ($n = 22$), randomized to hypoxia (FiO_2 0.08, H, $n = 16$) or normoxia (FiO_2 0.21, C21, $n = 6$) for 120 min. The hypoxia group was further randomized to subsequent reoxygenation for 30 min with FiO_2 0.21 (H21, $n = 8$) or 1.00 (H100, $n = 8$). Following 150 min survival in air, pups were returned to their dam for observation before they were euthanized postexperimental day 3. There was no necrosis in the HE–stained slides in any of the regions of interest: hippocampus, striatum, or cortex, but sparse apoptosis. Apoptotic cells (i.e., cells showing condensation and fragmentation of the nucleus and eosinophilic cytoplasm) were identified by light microscopy at high magnification ($\times 400$) and ranged from one to nine in number in each regions of interest of the three groups. No significant differences were observed between intervention groups and controls. We performed IHC with the microglial marker Iba1 (ionized calcium-binding adapter molecule 1) and the astrocytic marker GFAP (glial fibrillary acidic protein). IHC showed a significantly increased number of Iba1⁺ cells in striatal tissue both in H21 $P = 0.004$ and in H100 $P = 0.014$ compared with controls (C21). In the CA1 area of hippocampus,

the number of Iba1⁺ cells was significantly increased when comparing both H21 $P = 0.009$ and H100 $P = 0.0002$ with controls (C21). In the CA2 area, comparison of H100 and C21 was significantly changed $P = 0.047$ (H21 vs. C21, $P = 0.099$). In CA3, only the difference between H21 and C21 was significant, $P = 0.031$ (H100 vs. C21, $P = 0.160$) (Figure 1). Densitometric quantification, i.e., the mean fluorescent intensity, of the GFAP signal in the striatum and the hippocampus did not reveal any significant changes between the three groups (H21, H100, and C21) (see Supplementary Table S1 online).

Microarray Analysis

On P7, 67 C57BL/6 mice from ten litters, each comprising 6–10 pups were assigned for gene expression analysis. Totally 11 mice were excluded, 8 died during hypoxia and 3 were excluded due to technical problems. Among the 56 included mice, there were no significant weight (hypoxia 3.9 ± 0.4 g, $n = 38$ vs. normoxia 3.9 ± 0.3 g, $n = 18$) or gender (30 female, 26 male) differences between the groups. The hypoxia group was further randomized to subsequent reoxygenation for 30 min with different FiO_2 (Figure 2).

In whole forebrain homogenates, 701 out of the 34,670 probe sets on the microarray chip were found to be differentially expressed in the four hypoxia groups (H21, H40, H60, and H100) compared with controls (C21). Among the 24,674 probe sets with known gene symbols, 458 genes were differentially expressed compared with controls (C21). The number of differentially expressed genes was further reduced by setting the cutoff criteria at fold change (FC) ≥ 1.2 or < 0.8 , ending at

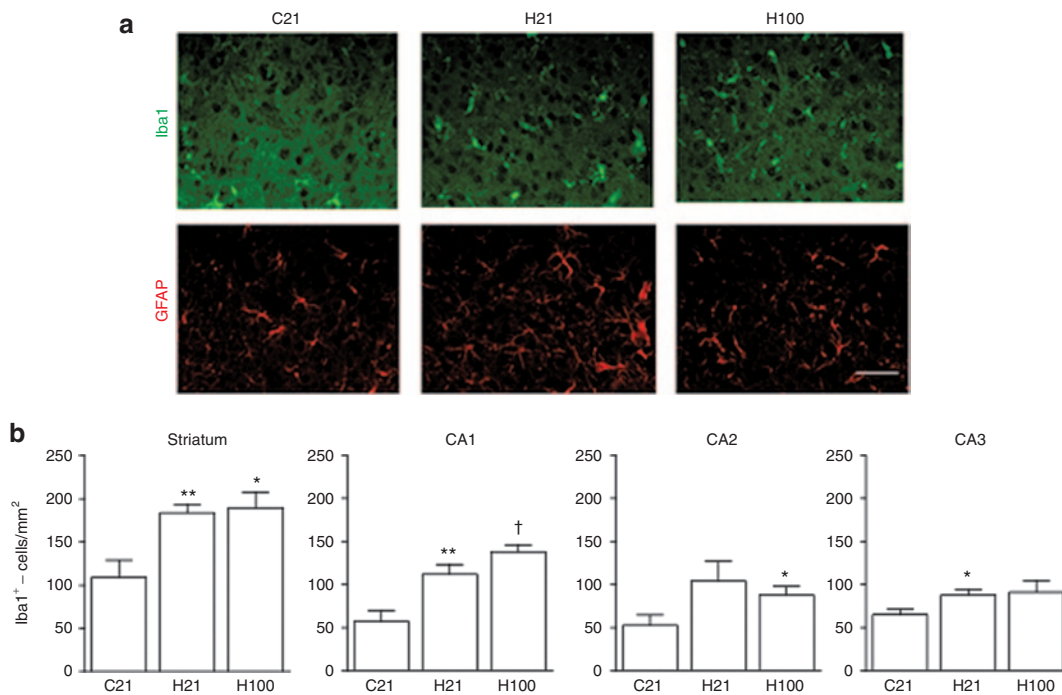


Figure 1. Immunohistological analysis. The microglial response after hypoxia–reoxygenation is increased compared with controls in striatum and hippocampus. (a) Illustration of microglia (Iba1⁺) and astrocytes (GFAP⁺) in striatal tissue 3 d after hypoxia–reoxygenation (bar = 50 μm). (b) Quantification of the total number of Iba1⁺ cells per square millimeter in striatum, CA1, CA2, and CA3 region of the hippocampus. Striatum: H21 vs. C21, ** $P = 0.004$ and H100 vs. C21, * $P = 0.014$. CA1: H21 vs. C21, ** $P = 0.009$ and H100 vs. C21, † $P = 0.0002$. CA2: H100 vs. C21, * $P = 0.047$. CA3: H21 vs. C21, * $P = 0.031$. GFAP, glial fibrillary acidic protein; Iba1, ionized calcium-binding adapter molecule 1.

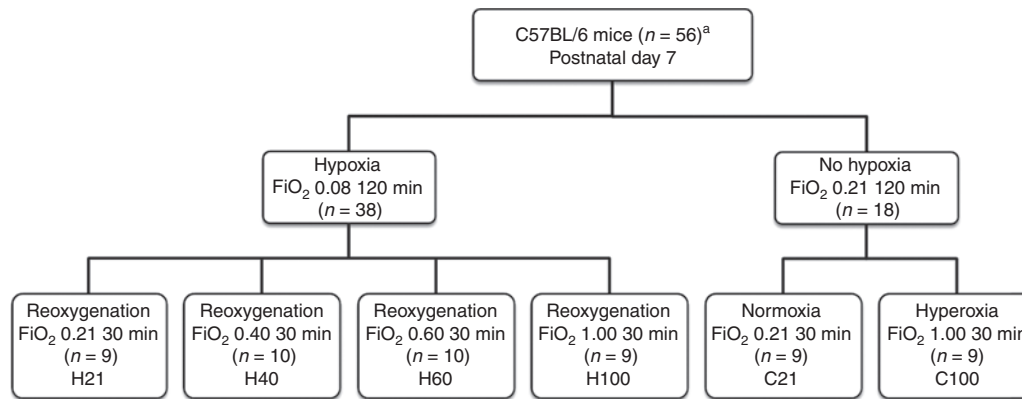


Figure 2. Experimental design and experimental groups. Clinically relevant statistical comparisons were performed between groups H21, H40, H60, H100, C21, and C100. ^aOut of 67 animals assigned to gene expression analysis, 8 animals died during hypoxia and 3 were excluded due to technical problems. FiO_2 , fraction of inspired oxygen.

201 genes. The distribution in the four hypoxia groups was as follows: H21 16.9%, H40 3.0%, H60 37.8%, and H100 42.3% (Figure 3a and Supplementary Table S2 online). Compared with reoxygenation with air (H21), the three groups receiving supplemental oxygen had differential expression of 934 of the 34,670 probe sets. 545 of the probe sets had known gene symbols and the number was further reduced by using cut-off criteria as above, ending at 141 genes distributed as follows: H40 0.7%, H60 27.7%, and H100 71.6% (Figure 3b and Supplementary Table S3 online).

Hypoxia induced three times more genes with differential expression when succeeded by supplemental oxygen (H100 vs. C100, 105 genes) rather than by air (H21 vs. C21, 34 genes) (Figure 3c and Supplementary Table S4 online). In comparison, twice the number of genes were responsive to 30 min of hyperoxia *per se* (C100 vs. C21, 178 genes) than to hypoxia followed by hyperoxia (H100 vs. C21 85 genes) in this model (Figure 3d and Supplementary Table S5 online). The cut-off criteria described above were also used for the two last sections.

Identification of Unique and Jointly Expressed Genes

Comprehensive analysis of the differentially expressed genes compared with control after cutoff criteria was applied revealed overlapping results between the hypoxia–reoxygenation groups. Genes were selected based on their pivotal functions (Figure 4a and Table 1). The highest number of jointly expressed genes was found between H60 and H100. The H40 group shared only a few genes with the three other hypoxia–reoxygenation groups (data not shown). When studying hypoxia followed by air (H21), hypoxia–reoxygenation with 100% O_2 (H100) and hyperoxia *per se* (C100), a distinct gene expression pattern appeared after hyperoxia alone compared with when hyperoxia was preceded by hypoxia (Figure 4b and Table 1).

Cluster Analysis

The expression patterns of transcripts that showed significant changes in at least one of the hypoxic groups compared with controls (C21) were hierarchically clustered. The heat map shows two major clusters consisting of up- and downregulated

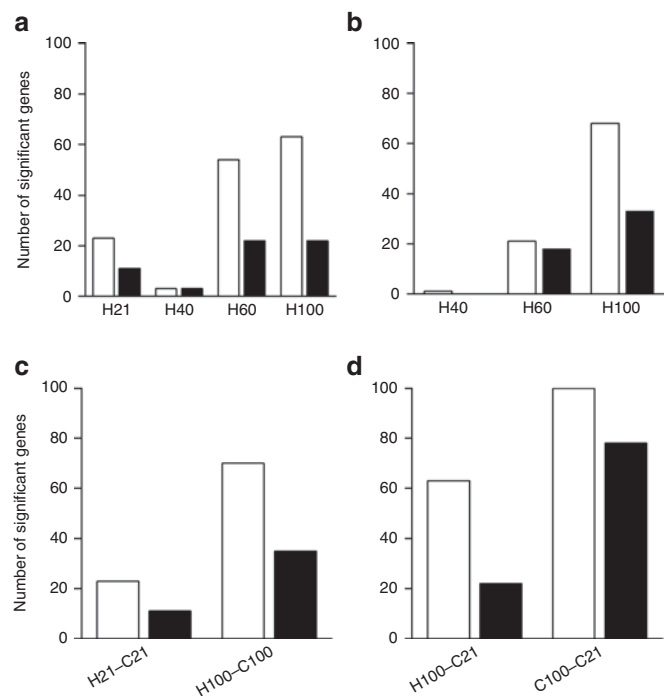


Figure 3. Overall gene expression. (a) BAMarray analysis: the number of differentially expressed probe sets with known gene symbol identified as up- (white bars) or downregulated (black bars) in the four different hypoxia groups, each of them compared with controls (C21) after cutoff fold change (FC) ≥ 1.2 or < 0.8 (also applied for b-d). (b) The number of differentially expressed probe sets with known gene symbol altered in mice reoxygenated with supplemental oxygen compared with mice reoxygenated with air (H21). (c) The effect of hypoxia during reoxygenation with either fraction of inspired oxygen (FiO_2) 0.21 or 1.00. (d) The effect of hypoxia followed by hyperoxic reoxygenation (H100 vs. C21) compared with hyperoxia *per se* (C100 vs. C21).

genes (Figure 5). Several subclusters were observed, which contained genes that displayed similar functions and gene expression changes. The H100 group displayed two pronounced subclusters of genes involved in inflammatory response, intracellular signaling, transcription, and nucleotide binding. In the downregulated major cluster, the H100 group displayed a subcluster with genes involved in metal ion binding.

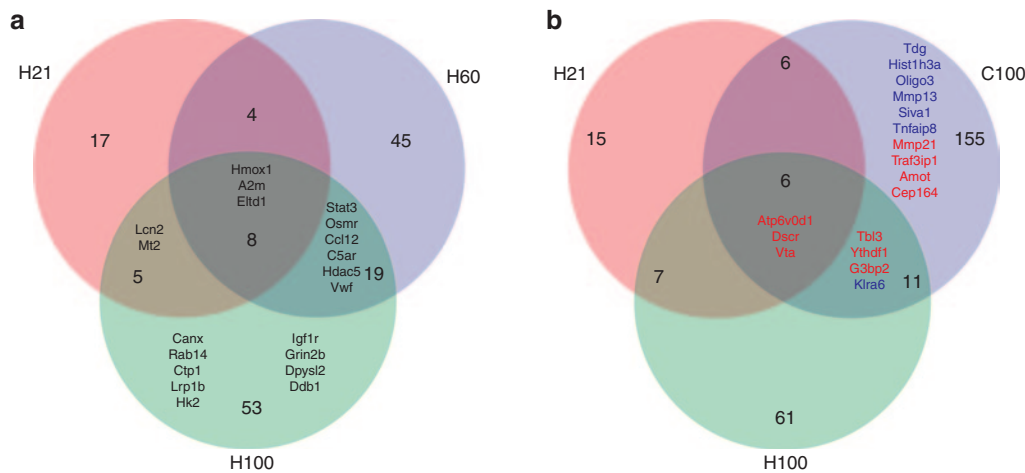


Figure 4. Unique and jointly expressed genes. Venn diagrams indicating the number of differentially, jointly, and uniquely expressed genes identified after BAMarray analysis followed by further cutoff fold change ≥ 1.2 or < 0.8 . The number of genes unique for each condition is expressed in the outer circle. Jointly expressed genes are denoted in the intersections of each condition, and gene expressions changed at all conditions are represented in the centered intersection of all circles. (a) The three hypoxia groups compared with controls (C21). Listed genes are upregulated. (b) Hypoxia followed by reoxygenation with fraction of inspired oxygen 0.21 (H21 vs. C21) or 1.00 (H100 vs. C21) and hyperoxia *per se* (C100 vs. C21). Listed genes are colored as red for upregulated and blue for downregulated. Full gene name for all genes can be found in [Table 1](#) and in [Supplementary Tables S1–S7](#) online.

Pathways and Functional Categories

Gene Set Enrichment Analysis (GSEA) was performed on the preprocessed and normalized data independently of the Bayesian ANOVA of microarrays (BAMarray) analysis and revealed seven significantly altered pathways on *a priori* selected gene sets with a chosen cutoff false discovery rate q value < 0.15 in six different comparisons ([Table 2](#)). Oxidative phosphorylation was the only enriched pathway significantly downregulated in both H60 and H100, and 48 out of the 104 genes were here repressed in both groups (see [Supplementary Table S6](#) online).

Validation of the Microarray Results

To validate the microarray data, seven transcripts were analyzed with RT-PCR in 39 of the same samples used in the microarray study ([Figure 6](#)). Pearson correlation coefficient (r) and belonging P value for the transcripts: *Hmox1*, *Stat3*, *Osmr*, *Igfr1*, *Mt2*, *Cox6a2*, and *Hdac5* ranged from 0.43 to 0.86 and from 0.03 to < 0.0001 , respectively.

DISCUSSION

In this study, we have performed microarray analysis on whole forebrain homogenates from P7 mice approximating the late preterm infant (16), to determine transcriptional activation or repression after hypoxia followed by reoxygenation with graded FiO_2 supplementation. Our hypoxia model resulted in physiological stress, demonstrated with significant metabolic acidosis (17) and cardiac and respiratory changes in line with the definition of intrapartum fetal asphyxia (18). A significant increase of microglial cells was observed after hypoxia–reoxygenation both in striatal tissue and in the hippocampal CA1, but with no differences between the reoxygenation regimes. The main finding of this study was that a considerably higher number of genes expressed in the brain were induced by hypoxia followed by 30 min of hyperoxic reoxygenation with 60 or 100% O_2 as

compared with those induced by 21 and 40% O_2 . Pathway analyzes showed downregulation of oxidative phosphorylation in the 60 and 100% O_2 groups, indicating a reduced production of high-energy phosphates and more severe primary energy failure when high levels of supplemental O_2 were used during resuscitation. When comparing the three hyperoxic groups with the group reoxygenated with air, a dose-dependent gene expression pattern was revealed. Hyperoxia *per se* defined a unique gene expression pattern compared with when hyperoxia was preceded by hypoxia, thus disclosing different transcriptional activations due to these distinct stimuli. Our aim was to mimic a global hypoxic insult followed by subsequent reoxygenation, to be able to study the sudden reintroduction of different FiO_2 to hypoxic brain tissue, as done previously (19). We therefore avoided ligation of the carotid artery as used in the Vanucci model, producing a focal brain injury. It is highly important to customize therapy after a hypoxia situation at birth followed by resuscitation in regard to insult severity and timing, which can be monitored both by imaging and biomarkers. The alteration of cell death pathways and response to neuroprotective strategies seem to have different effects on focal vs. global hypoxia (20), with the latter being independently able to induce oxidative injury in the cerebral cortex (21). Nevertheless, the hypoxia–reoxygenation model is a milder oxidative insult than HI, and there is evidence that this hypoxia-provoked oxidative stress can be counteracted by central nervous system protective mechanisms (22). However, the antioxidant defenses can be overcome in a hypoxia–reoxygenation model, depending on the intensity and/or duration of the oxidative stress (23). In the current model, we observed no neuronal cell death in any examined region: cortex, striatum, or hippocampus. This is in line with Weber *et al.* (24) who reported no increase in neuronal death even after 8% O_2 for two 8-h periods in the newborn rat brain. Our group has shown that 100% O_2 increases the extent of cerebral injury when

Table 1. Genes jointly expressed in different statistical comparisons, and genes unique for singular statistical comparisons

Gene name	Gene symbol	Function	Statistical comparison			
			H100–C21	H60–C21	H21–C21	C100–C21
Adenomatosispolyposis coli	<i>Apc</i>	Tumor suppressor				
Alpha-2-macroglobulin	<i>A2m</i>	Acute phase protein	1.4	1.3	1.4	
Angiomotin	<i>Amot</i>	Angiogenesis				1.2
Angiopoietin 2	<i>Angpt2</i>	Angiogenesis			1.3	
Apelin	<i>Apc</i>	Oxidative stress				
B-cell linker	<i>Blnk</i>	Oxidative stress				
Calnexin	<i>Canx</i>	Chaperone	1.7			
Centrosomal protein 164	<i>Cep164</i>	Cell cycle				1.2
Chemokine ligand 12	<i>Ccl12</i>	Chemokine	1.5	1.6		
Complement component 5a receptor 1	<i>C5ar1</i>	Inflammation	1.3	1.4		
C-terminal binding protein 1	<i>Ctp1</i>	Transcription	1.5			
Damage-specific DNA binding protein 1	<i>Ddb1</i>	DNA repair	1.2			
Dihydropyrimidinase-like 2	<i>Dpsyl</i>	Immunity	1.2			
EGF, latrophin seven transmembrane domain 1	<i>Eldt1</i>	Unknown	1.4	1.4	1.6	
Glutamat receptor 2b	<i>Grin 2b</i>	Excitotoxicity	1.2			
Heme oxygenase 1	<i>Hmox1</i>	Stress defense	1.6	1.9	1.6	
Hexokinase 2	<i>Hk2</i>	Glycolysis	1.3			
Histone cluster 1 H3a	<i>Hist1h3a</i>	Cell cycle				0.7
Histone deacetylase 5	<i>Hdac5</i>	Transcription	1.6	1.6		
Insulin-like growth factor 1 receptor	<i>Igf1r</i>	Development	1.2			
Lipocalin 2	<i>Lcn2</i>	Inflammation	1.5		1.6	
Low density lipoprotein related protein 1	<i>Lrp1b</i>	Neurodevelopment	1.5			
Matrix metalloproteinase 13	<i>Mmp13</i>	Angiogenesis				0.8
Matrix metalloproteinase 21	<i>Mmp21</i>	Tumor progression				1.3
Metallothionein 1	<i>Mt1</i>	Stress defense			1.5	
Metallothionein 2	<i>Mt2</i>	Stress defense	1.8		2.1	
Oligodendrocyte transcription factor 3	<i>Oligo3</i>	Transcription				0.8
Oncostatin M receptor	<i>Osmr</i>	Inflammation	1.4	1.4		
RAB14, member RAS oncogene family 14	<i>Rab14</i>	Vesicular trafficking	1.8			
Serine peptidase inhibitor 3	<i>Serpina3</i>	Protease inhibition			1.7	
Signal transducers and activators of transcription protein 3	<i>Stat3</i>	Transcription factor	1.3	1.3		
SIVA apoptosis- inducing factor pseudogene 1	<i>Siva1</i>	Apoptosis				0.8
Thymine DNA glycosylase	<i>Tdg</i>	DNA repair				0.7
TRAF3 interacting protein 1	<i>Trafip1</i>	Signal transduction				1.3
Tumor necrosis factor, alpha induced protein 8	<i>Tnfaip8</i>	Apoptosis				0.8
Von Willebrand factor	<i>Vwf</i>	Inflammation	1.2	1.2		

Numbers in space are fold change values. Blank spaces indicate nonsignificance.

administered to hypoxemic piglets or rats (8,25). Felderhoff-Mueser *et al.* (26) even report that 80% O₂ without preceding hypoxia induces cell death after a 2-h exposure in the newborn brain. Despite the lack of neuronal cell death, a microglial accumulation was observed here 3 d after hypoxia–reoxygenation. In the developing brain, microglial cells respond rapidly to any kind of central nervous system pathology, but the

degree of activation depends on the severity of the damage as reviewed by Vexler and Yenari (6). Our data show increased accumulation of microglia (Iba1⁺ cells) in striatum and hippocampal CA1, irrespective of which reoxygenation regime was applied (21 or 100% O₂). In contrast to these findings, a study in adult rats shows significantly increased Iba1⁺ cells in CA1 after 100% O₂ reoxygenation compared with 21% O₂

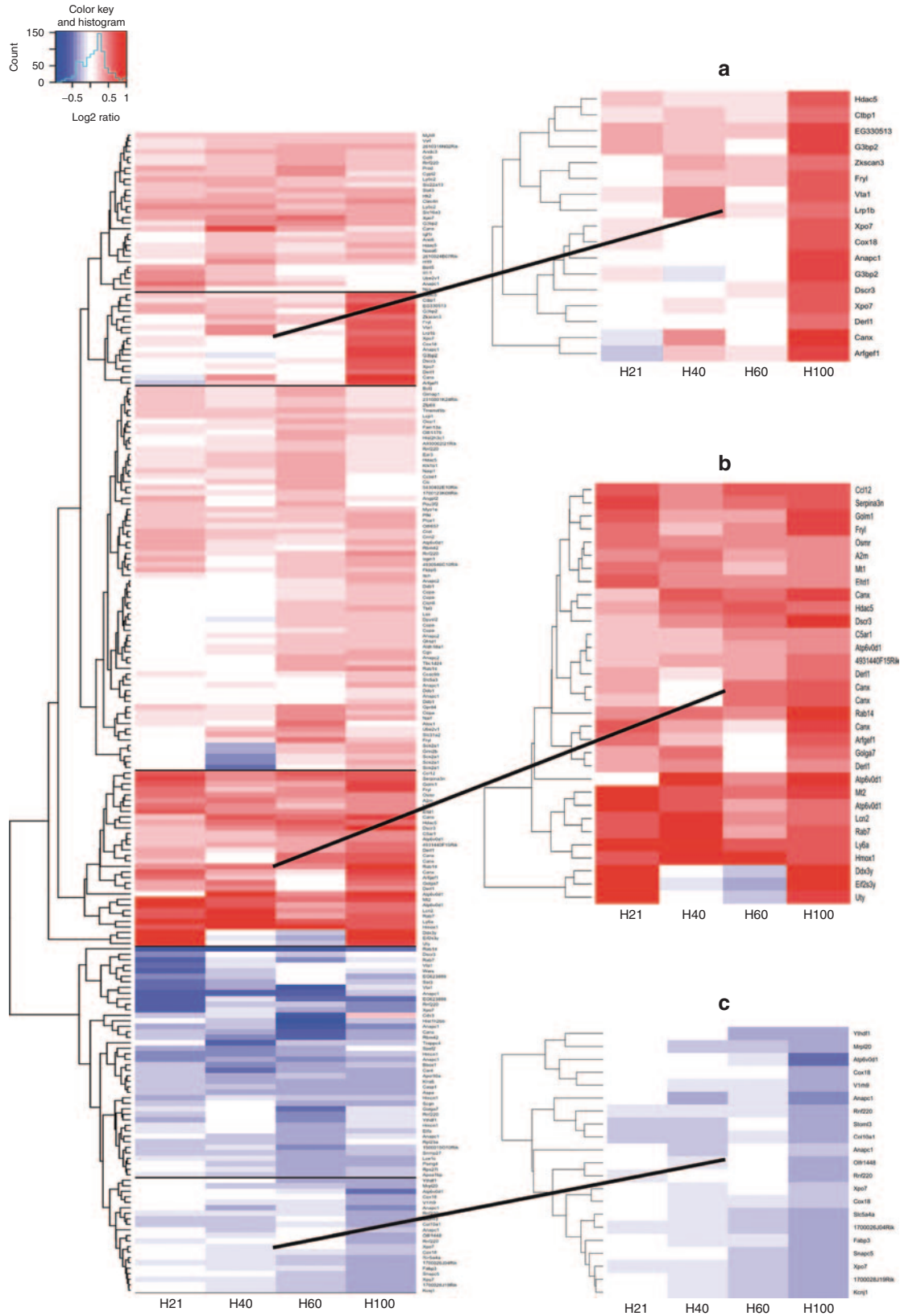


Figure 5. Cluster analysis. Significantly differentially expressed transcripts were clustered according to similarity in fold change expression in the four hypoxia groups vs. controls (C21). Red represents upregulation and blue represents downregulation. The color key indicates the degree of regulation in the range of the given values. **(a,b)** The H100 group displayed two pronounced subclusters among the upregulated transcripts, with genes mainly involved in inflammatory response, intracellular signaling, transcription, and nucleotide binding. **(c)** Downregulation, including genes involved in metal ion binding.

Table 2. Pathway analysis with FDR q value <0.15

Database	Pathways	Statistical comparison ^a	Type of regulation	FDR q value	NES
KEGG	DNA replication	H21–C21	Downregulated	0.108	–1.60
		H60–C21	Downregulated	0.144	–1.57
	RNA polymerase	H40–C21	Downregulated	0.143	–1.53
	Oxidative phosphorylation	H60–C21	Downregulated	0.073	–1.57
		H100–C21	Downregulated	0.117	–1.64
Gene Ontology	Activation of NF- κ B transcription factor	H21–C21	Upregulated	0.005	2.03
	Damaged DNA binding	H40–C21	Downregulated	0.047	–1.87
	Cell structure disassembly during apoptosis	H60–H21	Downregulated	0.125	–1.82
	Epidermal growth factor receptor signaling	H100–H21	Downregulated	0.089	–1.87

FDR, false discovery rate; KEGG, Kyoto Encyclopedia of Genes and Genomes; NES, normalized enrichment score.

^aStatistical comparison of group pairs.

following global cerebral ischemia 7 d after insult (27). Since we aimed for a milder oxidative insult, proliferation of microglia increased in a more modest manner as compared with HI in the immature brain (28). Astrocytes are affected by microglia activation after HI, contributing to excessive release of inflammatory mediators which can further intensify the injury (5). However, no significant changes in astrocytes density or cell death were observed after hypoxia–reoxygenation, suggesting that exposure to modest stimuli triggers the protective mechanisms that microglia possess (29). Different signaling molecules can stimulate microglia proliferation, many of these are directly involved in inflammatory responses e.g., cytokines, complement factors, chemokines, and toll-like receptors (5). In the current model, transcripts which were significantly increased in the microarray analysis were both pro- and anti-inflammatory. In general, the hypoxia–reoxygenation model induced modest differences in the expression of the majority of genes, measured as a FC ranging between 1.1 and 1.5. The expression of only a few genes was twofold increased. The rationale for including genes displaying such subtle alterations in expression levels is based on the knowledge that these genes can be of importance because of their biological function and involvement in complex pathways. Indeed, it has been shown that even a 20% difference in gene expression can be clinically significant (30). Transcriptional studies on global hypoxia and HI use different cutoff criteria, but both detect inflammatory-responsive genes (31,32). Moreover, hyperoxic reperfusion can trigger additional inflammatory response after hypoxia (7).

Inflammatory Responsive Genes

The hypoxia–reoxygenation model upregulated among others heme oxygenase 1 (*Hmox1*), lipocalin 2 (*Lcn2*), metallothionein 2 (*Mt2*), complement component 5a receptor 1 (*C5ar1*), chemokine (C-C motif) ligand 12 (*Ccl12*), signal transducer and activator of transcription 3 (*Stat 3*), oncostatin M receptor (*Osmr*), and Von Willebrand factor (*Vwf*) which can act pro- or anti-inflammatory. Microglial cells are activated in a graded response to central nervous system stimuli involving secretion or expression of cytokines and chemokines,

complement factors, and other inflammatory mediators (5). Herein, most expression changes in regards to inflammation were identified after hyperoxic reoxygenation with 60 or 100% O₂, while microglial accumulation was observed in striatum and hippocampal CA1 independently of which reoxygenation regime being applied (21 or 100% O₂). Since the expression data are based on whole forebrain homogenates in contrast to the IHC performed in brain subregions, this can explain the more modest inflammatory response observed after hypoxia followed by air.

Oxidative Phosphorylation and Hyperoxic Reoxygenation

Pathway analysis by GSEA of the normalized data identified biochemical and functional pathways with altered transcription. In particular, the oxidative phosphorylation pathway was downregulated after reoxygenation with both 60 and 100% O₂. Downregulated genes were found in each of the five complexes constituting this pathway (complex I–V). Hypoxia and/or ischemia may both lead to inadequate supplies of glucose and oxygen, followed by dose-dependent depletions of high-energy phosphates (2). Hyperoxic reoxygenation further impairs the oxidative energy metabolism in subregions of the brain (33). In line with these findings, our group has shown a slower decline in Krebs cycle intermediates in newborn pigs exposed to hypoxia followed by reoxygenation with 100% O₂ (34). Moreover, epidermal growth factor receptor (*Egfr*) signaling pathway was also downregulated after using 100% O₂ compared with when room air was applied during reoxygenation. Prolonged activation of *Egfr* may trigger oxidative neuronal injury in central neurons (35), and suppression of this pathway may be a protective response to hyperoxia.

Excitotoxicity and Repair After Hyperoxic Reoxygenation

The ionotropic glutamate receptor NMDA2B (*Grin2b*), insulin-like growth factor I receptor (*Igfr1r*), and damage-specific DNA binding protein 1 (*Ddb1*) are among the genes responding to reoxygenation with 100% O₂. Overactivation of *Grin2b* is linked to impairment of glutamate uptake by glia (3). As shown herein, co-expression with *Mt2* can be indicative of

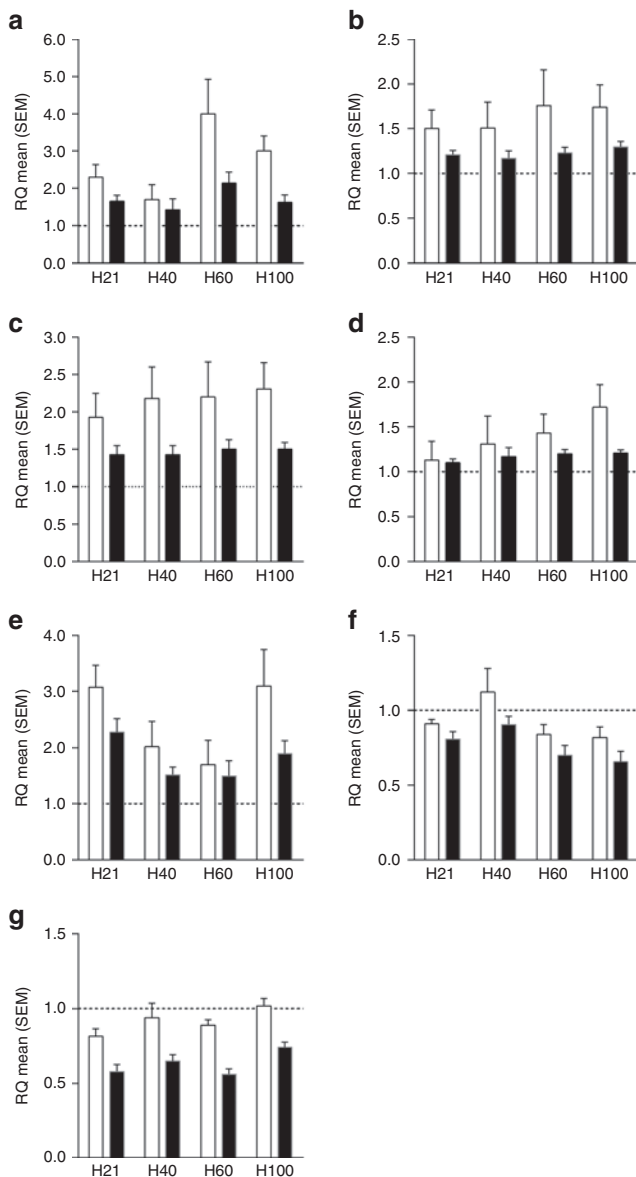


Figure 6. Validation of microarray results by RT-PCR. Relative quantification (RQ) signal levels of seven selected transcripts determined by microarray (black bars) compared with levels as determined by RT-PCR (white bars). (a–g) The data are expressed as mean fold change and the error bars are SEM for each hypoxia group (H21, H40, H60, and H100) compared with controls (C21, dotted line). Pearson correlation coefficient and belonging *P* value are calculated for each gene. (a) *Hmxo1* ($r = 0.74$; $P < 0.0001$), (b) *Stat3* ($r = 0.64$; $P = 0.0001$), (c) *Osmr* ($r = 0.48$; $P = 0.007$), (d) *Igfr1* ($r = 0.79$; $P < 0.0001$), (e) *Mt2* ($r = 0.86$; $P < 0.0001$), (f) *Cox6a2* ($r = 0.76$; $P < 0.0001$), and (g) *Hdac5* ($r = 0.43$; $P = 0.03$).

excitotoxic injury. A recent study has demonstrated *Mt1/Mt2* to provide protection against NMDA receptor-mediated oxidative injury (36). *Igfr1r* functions as the receptor for *Igfl*. Increased *Igfl* can be produced by microglia after injury in a repair process being supportive and anti-inflammatory (6), and no neuronal cell death was observed in the current model. Furthermore, *Ddb1* is active in nucleotide excision repair of bulky, shape-distorting lesions in the DNA double helix. Bulky oxidative DNA lesions rapidly accumulate in

liver and kidney tissue of rats after normal birth, consistent with oxidative stress induced by the sudden increase in partial oxygen pressure (37). Increased *Ddb1* might reflect effects of supplementary oxygen on the integrity of DNA, although the collective DNA damage response and immediate counteraction of damage is orchestrated by posttranslational protein modifications (38). Hyperoxia *per se* activated a unique gene expression pattern compared with when hyperoxia was preceded by hypoxia. Hypoxia and hyperoxia are the extremes in regards of oxygen availability and can induce cell death independently (8,26). Herein, hypoxia followed by 100% O_2 orchestrated several genes overlapping with the other hypoxia groups, while the gene profile induced by hyperoxia *per se* differed, calling for other underlying mechanisms.

Limitations of the Study

The current study was restricted to analysis of mRNA expression levels, without measurements of the actual protein levels or enzymatic activities. Moreover, gene expression was studied at one early time point, revealing only the acute affection on gene expression after hypoxia–reoxygenation. We are currently performing a follow-up study with temporal gene and protein expression profiling.

Conclusion

Reoxygenation with 60 or 100% O_2 increases brain inflammatory gene expression and decreases expression of genes involved in oxidative phosphorylation pathway in the immature brain. A hypoxia–reoxygenation event accumulates microglial proliferation in selective vulnerable subregions of the brain. The acute transcriptional changes may be of concern after using supplementary oxygen, as long-term consequences cannot be ruled out. Further studies can add additional insights into the mechanisms of the identified genes and pathways related to hypoxia–reoxygenation in the newborn brain.

METHODS

Animals

All experiments were approved by the Norwegian Animal Research Authority. The animals were cared for and handled in accordance with the European Guidelines for Use of Experimental Animals by FELASA (Federation of European Laboratory Animals Science Association) researchers. C57BL/6 mice were received from the Taconic Facility in Tornbjerg, Denmark. Mice were stabled and bred at 24 °C on a 12:12 light/dark cycle with access to a diet of pellets and water *ad libitum*. All experiments were performed on P7 mice (day of discovery was counted as day 1).

Hypoxia and Reoxygenation Model

Custom-made Lucite chambers were used for hypoxia and reoxygenation experiments. Hypoxia was performed with premixed gas: 8% oxygen balanced in nitrogen (Yara, Oslo, Norway). Following hypoxia, reoxygenation with different FiO_2 levels (0.21, 0.40, 0.60, and 1.00) was performed simultaneously in separate chambers. During reoxygenation, FiO_2 was monitored with conventional oxygen mixers. Constant atmospheric pressure was maintained by a continuous supply of 0.5 l/min and open outlets. CO_2 concentrations were $<0.3\%$. The temperature in the chambers was kept constant at 35 ± 0.5 °C by floor heating and humidity was maintained at 40–50% with an open water source. Pups were separated from their dams throughout the experiment. Mice were not anesthetized or restrained.

Validation of the Model

Morphology. To validate the hypoxia–reoxygenation model, hematoxylin and eosin staining and immunohistochemical analysis were performed in P7 mice from four litters ($n = 22$), randomized to hypoxia (FiO₂ 0.08, H, $n = 16$) or normoxia (FiO₂ 0.21, C21, $n = 6$) for 120 min. The hypoxia group was further randomized to subsequent reoxygenation for 30 min with FiO₂ 0.21 (H21, $n = 8$) or 1.00 (H100, $n = 8$). Following 150-min survival in air, pups were returned to their dam for observation. After 3 d, mice were anesthetized with a single dose of fentanyl/fluanisone and midazolam subcutaneously and transcardially perfused with phosphate-buffered saline followed by 4% paraformaldehyde. Coronal tissue blocks (0.5-cm thick) were dehydrated, embedded in paraffin, and sliced into 4- μ m thick sections. To determine apoptosis and/or necrosis, a pathologist blinded to the experimental groups assessed hematoxylin and eosin–stained brains in the regions of interest: hippocampus, cortex, and striatum. Immunostaining was performed as previously described (28). The primary antibodies and dilutions used were mouse anti-GFAP 1:400 (G3893; Sigma, St. Louis, MO) and rabbit anti-Iba1 1:2000 (019-19741, Wako, Richmond, VA). Secondary antibodies were Alexa Fluor 594 (A11005) and Alexa Fluor 488 (A11008) (Invitrogen, Grand Island, NY), both used in a 1:5,000 dilution. For negative control staining, normal mouse and rabbit IgG were used as primary antibodies. Images of the slides were captured using a Nikon Eclipse E400 (Nikon Instruments, Melville, NY). Two predetermined regions from striatum and three from hippocampus (CA1, CA2, and CA3) were captured under identical settings. All images were processed and quantified using ImageJ 1.42q software (National Institutes of Health, Bethesda, MD). Densitometric measurements by ImageJ were used for identifying GFAP⁺ cells, and manually cell counting was applied for Iba1⁺ cells, which were counterstained with 4',6-diamidino-2-phenylindole (Sigma) for identification.

Microarray Experiment

Sixty-seven P7 mice from 10 different litters were randomized to hypoxia or normoxia for 120 min. Eight died during hypoxia and three were excluded due to technical problems and finally 56 were included in the analysis. The hypoxia group was further randomized to subsequent reoxygenation for 30 min with FiO₂ 0.21 (H21, $n = 9$), 0.40 (H40, $n = 10$), 0.60 (H60, $n = 10$), or 1.00 (H100, $n = 9$), whereas the normoxia group was randomized to either FiO₂ 0.21 (C21, $n = 9$) or 1.00 (C100, $n = 9$). Following 150 min of survival in air, decapitation and rapid dissection on ice was performed. The olfactory bulb and the cerebellum were removed, and the forebrain was subsequently preserved in RNA later stabilization reagent at -20°C (Qiagen, Hilden, Germany). RNA extraction was performed as described previously (17).

Microarray Analysis

One hundred nanograms of total RNA was used for each of the 56 microarray experiments, using Mouse Gene 1.0 ST Arrays (Affymetrix, Santa Clara, CA) containing 750,000 unique 25-mer oligonucleotides constituting over 28,000 gene-level probe sets. Microarray analysis was performed according to the manufacturer's protocol (GeneChip Whole Transcript sense Target Labeling Assay Manual, version 4), and described previously (17). For further statistical analysis, *.cel files generated by GeneChip Operating Software (Affymetrix) were used (see **Supplementary Methods** online).

Primer Design and Real-Time RT-PCR

RT-PCR was performed on the 39 samples (H21; $n = 8$, H40; $n = 6$, H60; $n = 7$, H100; $n = 9$, C21; $n = 9$) with sufficient cDNA left, to verify the differentially expressed transcripts detected by microarray. Primers were designed for each transcript (*Hmox1*, *Stat3*, *Osmr*, *Igf1r*, *Mt2*, *Cox6a*, and *Hdac5*) using Primer Express 3.0 Software (Applied Biosystems, Grand Island, NY) (see **Supplementary Table S7** online). Total mRNA was extracted, reverse transcribed, amplified, and analyzed as described previously (17). Briefly, RT-PCR was performed with 50 ng of cDNA and 400 nmol/l primers for the target genes and reference gene PPIA (peptidylprolyl isomerase A). Data were analyzed by the comparative Ct method of relative quantification (RQ) ($2^{-\Delta\Delta\text{Ct}}$). Cycle threshold (Ct) values of the target transcripts

were normalized to Ct values of the PPIA gene in the same sample, resulting in ΔCt Sample. ΔCt calibrator was calculated from the average ΔCt in the nine controls in the C21 group. RQ is defined as $2^{-\Delta\Delta\text{Ct}}$, where $\Delta\Delta\text{Ct} = \Delta\text{Ct sample} - \Delta\text{Ct calibrator}$.

Statistical Analysis

A two-tailed *t*-test was used in the validation experiment of the model. Pearson correlation was used to examine the correlation between the RT-PCR and microarray results, using FC relative to mean of C21 group for each individual. GraphPad Prism versions 5.01 and 6.01 (Graph Pad Software, San Diego, CA) were used for designing graphs and calculations.

The microarray data were preprocessed using the R/Bioconductor package Robust Multiarray Average (RMA) (Fred Hutchinson Cancer Research Center, Seattle, WA) as previously described (17). In RMA, raw intensity values are background corrected, log₂ transformed and then quantile normalized, before an additive linear model is applied to the normalized data. The results are an expression measure for each probe set on each array. Arrays were preprocessed together to ensure comparability across conditions.

The BAMarray method was used to identify differentially expressed genes as previously described (17). This method balances the number of falsely detected genes and falsely nondetected genes, i.e., it controls both the false discovery rate and the false nondiscovery rate. The cutoff value that results in an optimal balance is determined automatically from the data, contrary to most other software packages that require the users to specify a cutoff value for the test statistic. In BAMarray, the expression values for all probe sets are taken into account and results in a list of differentially expressed probe sets or genes as indicated by their known gene symbol. To reduce the number of genes to be further studied, cutoff criteria was set at FC ≥ 1.2 or < 0.8 .

In the cluster analysis, genes were clustered according to similarity in expression values. Average FC for genes being significantly expressed in at least one of the four hypoxia groups vs. controls (C21) were clustered using Pearson correlation as distance measure.

GSEA is a method to determine whether a set of *a priori* defined gene sets is significantly enriched in one group compared with another and was applied as earlier described (17). The GSEA analysis was performed for the probe sets with known gene symbol only, and the median of the probe set intensities was used for probes sharing gene symbols. The gene sets were selected among the Gene Ontology and Kyoto Encyclopedia of Genes and Genomes pathway database (KEGG) gene sets available in the Molecular Signatures Database (MSigDB v2.5). A weighted Kolmogorov–Smirnov-like statistic was calculated for each gene set, and statistical significance was assessed by permutation tests. To adjust for multiple hypotheses testing when several gene sets are considered, the false discovery rate is controlled.

All microarray data are MIAME compliant and the following link has been created to allow review of the data in Gene Expression Omnibus (GSE32500).

SUPPLEMENTARY MATERIAL

Supplementary material is linked to the online version of the paper at <http://www.nature.com/pr>

ACKNOWLEDGMENTS

We express gratitude to Monica Atneosen-Aasegg and Grethe Dyrhaug for their assistance during the animal experiments and RT-PCR. We thank Jonas Øgaard and Grethe Dyrhaug for valuable contribution in the immunohistological analysis. The animal experiments were performed at Centre of Comparative Medicine, Oslo University Hospital, Rikshospitalet, and we appreciate the help and facilities that we were offered during our work.

STATEMENT OF FINANCIAL SUPPORT

This study was supported by Financial Mechanism of European Economic Area (PL0226), Polish Ministry of Science (E023/P01/2008/02/85), and South-Eastern Regional Health Authority, Norway.

Disclosure: The authors declare no conflicts of interest.

REFERENCES

- Boschi-Pinto C, Young M, Black RE. The Child Health Epidemiology Reference Group reviews of the effectiveness of interventions to reduce maternal, neonatal and child mortality. *Int J Epidemiol* 2010;39:Suppl 1:i3–6.
- Vannucci RC, Yager JY, Vannucci SJ. Cerebral glucose and energy utilization during the evolution of hypoxic-ischemic brain damage in the immature rat. *J Cereb Blood Flow Metab* 1994;14:279–88.
- Ferriero DM. Neonatal brain injury. *N Engl J Med* 2004;351:1985–95.
- McQuillen PS, Ferriero DM. Selective vulnerability in the developing central nervous system. *Pediatr Neurol* 2004;30:227–35.
- Vexler ZS, Tang XN, Yenari MA. Inflammation in adult and neonatal stroke. *Clin Neurosci Res* 2006;6:293–313.
- Vexler ZS, Yenari MA. Does inflammation after stroke affect the developing brain differently than adult brain? *Dev Neurosci* 2009;31:378–93.
- Markus T, Hansson S, Amer-Wählin I, Hellström-Westas L, Saugstad OD, Ley D. Cerebral inflammatory response after fetal asphyxia and hyperoxic resuscitation in newborn sheep. *Pediatr Res* 2007;62:71–7.
- Munkeby BH, Børke WB, Bjørnland K, et al. Resuscitation with 100% O₂ increases cerebral injury in hypoxic piglets. *Pediatr Res* 2004;56:783–90.
- Solberg R, Løberg EM, Andresen JH, et al. Resuscitation of newborn piglets. short-term influence of FiO₂ on matrix metalloproteinases, caspase-3 and BDNF. *PLoS ONE* 2010;5:e14261.
- Gill MB, Bockhorst K, Narayana P, Perez-Polo JR. Bax shuttling after neonatal hypoxia-ischemia: hyperoxia effects. *J Neurosci Res* 2008;86:3584–604.
- Ramji S, Ahuja S, Thirupuram S, Rootwelt T, Rooth G, Saugstad OD. Resuscitation of asphyxial newborn infants with room air or 100% oxygen. *Pediatr Res* 1993;34:809–12.
- Saugstad OD, Ramji S, Irani SF, et al. Resuscitation of newborn infants with 21% or 100% oxygen: follow-up at 18 to 24 months. *Pediatrics* 2003;112:296–300.
- Tan A, Schulze A, O'Donnell CP, Davis PG. Air versus oxygen for resuscitation of infants at birth. *Cochrane Database Syst Rev* 2005;<Volume>:CD002273.
- Perlman JM, Wyllie J, Kattwinkel J, et al.; Neonatal Resuscitation Chapter Collaborators. Part 11: Neonatal resuscitation: 2010 International Consensus on Cardiopulmonary Resuscitation and Emergency Cardiovascular Care Science With Treatment Recommendations. *Circulation* 2010;122(Suppl 2):S516–38.
- Raju TN, Higgins RD, Stark AR, Leveno KJ. Optimizing care and outcome for late-preterm (near-term) infants: a summary of the workshop sponsored by the National Institute of Child Health and Human Development. *Pediatrics* 2006;118:1207–14.
- Hagberg H, Peebles D, Mallard C. Models of white matter injury: comparison of infectious, hypoxic-ischemic, and excitotoxic insults. *Ment Retard Dev Disabil Res Rev* 2002;8:30–8.
- Wollen EJ, Sejersted Y, Wright MS, et al. Transcriptome profiling of the newborn mouse lung after hypoxia and reoxygenation: hyperoxic reoxygenation affects mTOR signaling pathway, DNA repair, and JNK-pathway regulation. *Pediatr Res* 2013;74:536–44.
- Low JA. Intrapartum fetal asphyxia: definition, diagnosis, and classification. *Am J Obstet Gynecol* 1997;176:957–9.
- Sejersted Y, Aasland AL, Bjørås M, Eide L, Saugstad OD. Accumulation of 8-oxoguanine in liver DNA during hyperoxic resuscitation of newborn mice. *Pediatr Res* 2009;66:533–8.
- Kofler J, Otsuka T, Zhang Z, et al. Differential effect of PARP-2 deletion on brain injury after focal and global cerebral ischemia. *J Cereb Blood Flow Metab* 2006;26:135–41.
- Solberg R, Longini M, Proietti F, Vezzosi P, Saugstad OD, Buonocore G. Resuscitation with supplementary oxygen induces oxidative injury in the cerebral cortex. *Free Radic Biol Med* 2012;53:1061–7.
- Sharp FR, Ran R, Lu A, et al. Hypoxic preconditioning protects against ischemic brain injury. *NeuroRx* 2004;1:26–35.
- Ezquer ME, Valdez SR, Seltzer AM. Inflammatory responses of the substantia nigra after acute hypoxia in neonatal rats. *Exp Neurol* 2006;197:391–8.
- Weber A, Dzierko M, Berns M, et al. Neuronal damage after moderate hypoxia and erythropoietin. *Neurobiol Dis* 2005;20:594–600.
- Dalen ML, Liu X, Elstad M, et al. Resuscitation with 100% oxygen increases injury and counteracts the neuroprotective effect of therapeutic hypothermia in the neonatal rat. *Pediatr Res* 2012;71:247–52.
- Felderhoff-Mueser U, Bittigau P, Siffringer M, et al. Oxygen causes cell death in the developing brain. *Neurobiol Dis* 2004;17:273–82.
- Hazelton JL, Balan I, Elmer GI, et al. Hyperoxic reperfusion after global cerebral ischemia promotes inflammation and long-term hippocampal neuronal death. *J Neurotrauma* 2010;27:753–62.
- Sejersted Y, Hildrestrand GA, Kunke D, et al. Endonuclease VIII-like 3 (Neil3) DNA glycosylase promotes neurogenesis induced by hypoxia-ischemia. *Proc Natl Acad Sci USA* 2011;108:18802–7.
- Carson MJ, Sutcliffe JG. Balancing function vs. self defense: the CNS as an active regulator of immune responses. *J Neurosci Res* 1999;55:1–8.
- Heidecker B, Kasper EK, Wittstein IS, et al. Transcriptomic biomarkers for individual risk assessment in new-onset heart failure. *Circulation* 2008;118:238–46.
- Gustavsson M, Wilson MA, Mallard C, Rousset C, Johnston MV, Hagberg H. Global gene expression in the developing rat brain after hypoxic preconditioning: involvement of apoptotic mechanisms? *Pediatr Res* 2007;61:444–50.
- Hedjtjärn M, Mallard C, Hagberg H. Inflammatory gene profiling in the developing mouse brain after hypoxia-ischemia. *J Cereb Blood Flow Metab* 2004;24:1333–51.
- Richards EM, Fiskum G, Rosenthal RE, Hopkins I, McKenna MC. Hyperoxic reperfusion after global ischemia decreases hippocampal energy metabolism. *Stroke* 2007;38:1578–84.
- Solberg R, Enot D, Deigner HP, et al. Metabolomic analyses of plasma reveals new insights into asphyxia and resuscitation in pigs. *PLoS ONE* 2010;5:e9606.
- Cha YK, Kim YH, Ahn YH, Koh JY. Epidermal growth factor induces oxidative neuronal injury in cortical culture. *J Neurochem* 2000;75:298–303.
- Yu X, Guo J, Fang H, Peng S. Basal metallothionein-I/II protects against NMDA-mediated oxidative injury in cortical neuron/astrocyte cultures. *Toxicology* 2011;282:16–22.
- Randerath E, Zhou GD, Randerath K. Organ-specific oxidative DNA damage associated with normal birth in rats. *Carcinogenesis* 1997;18:859–66.
- Huen MS, Chen J. The DNA damage response pathways: at the crossroad of protein modifications. *Cell Res* 2008;18:8–16.